3D Scalar Microwave Image Reconstruction Algorithm

Paul M. Meaney, Qianqian Fang, Shireen D. Geimer, Anatoly V. Streltsov, Keith D. Paulsen

Thayer School of Engineering, Dartmouth College, Hanover, NH 03755 USA

Abstract — **We have recently implemented a microwave imaging algorithm which incorporates scalar 3D wave propagation while reconstructing a 2D dielectric property profile. This is a preliminary step in reaching a full 3D image reconstruction approach but allows us to investigate important issues associated with speed of reconstruction and problem size. Key concepts developed during our 2D system evaluations have also proved to be translatable to the 3D approach and have accelerated the overall implementation.**

I. INTRODUCTION

Three dimensional microwave imaging for medical applications has long been a goal in the electromagnetics community but is fundamentally limited by the size of the region that can be interrogated and the time required to reconstruct an image [Caorsi et al., 1995; Semenov et al., 1999]. Two dimensional TM approaches have been implemented for phantom, animal and patient imaging exams with some success, especially when the imaging region is small [Meaney et al. 2001a]; however, artifacts are present which are most likely attributable to the 3D nature of the wave propagation. We have implemented a new algorithm, which is an important preliminary step towards full 3D imaging but may also provide immediate dividends in terms of improving our 2D imaging capabilities. This first step utilizes a scalar version of the wave equation in 3D and then reconstructs the object electrical properties as a 2D distribution. These initial steps towards a full 3D system are driven largely by microwave hardware and computational cost limitations. While not ideal, this study will facilitate assessment of the most significant 3D artifact contributors.

In terms of improving thermal imaging capabilities, the most notable limitation of our 2D system is the recovery of the conductivity component. The conductivity of some biological tissues at microwave frequencies can vary as much as 4 % per °C. Degradation of this image component will necessarily reduce thermal monitoring capability. For breast examinations, the breast is a high contrast, non-cylindrical scattering object with respect to various background media. We have estimated the effective imaging slice thickness to be roughly 3 —4 cm depending on the operating frequency and breast/background medium contrast [Meaney et al. 2001a]. Accounting for 3D wave propagation effects may reduce this slice thickness and improve tumor localization.

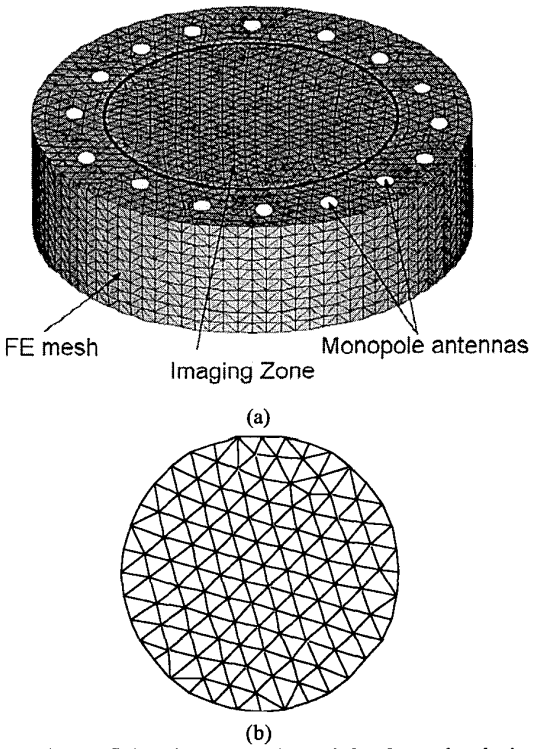

Fig. 1. (a) 3D finite element mesh used for forward solution calculation during the reconstruction, (b) 2D reconstruction parameter mesh (superimposed over imaging zone).

II. IMPLEMENTATION

Our approach is a Gauss-Newton iterative technique that minimizes the difference between the measured and computed field values and updates the property distribution (the image) until the difference is minimized. The computed field values are calculated on a 3D finite element mesh (10571 nodes and 54720 tetrahedral elements) in the shape of a short cylinder with a radius of 9 cm and height of 10 cm (Figure 1a). There are 16 vertically oriented monopole antennas spaced evenly on a circle of radius 7 cm that act as both transmitters and

0-7803-7239-5/02/$10.00 © 2002 IEEE

receivers. The imaging zone is a cylinder of 6 cm radius with an outer region having constant electrical properties of ε_r =77 and σ=1.7°S/m. A radiation boundary condition is applied on all surfaces of the larger cylinder. This configuration reflects our current 2D clinical implementation [Meaney et al. 2000]. In addition, the property distribution is recovered on 2D FE mesh (126 nodes and 214 triangular elements) that is discretized more coarsely than the 3D forward solution mesh and is superimposed over the imaging zone within the 3D mesh [Paulsen et al. 1995] (Figure 1b). The image is reconstructed on this smaller mesh to both restrict the size of the reconstruction problem and limit the amount of measurement data required.

III. Results

A. *Proof of Concept*

A number of simple experiments were performed to validate this implementation. In the first experiment, a 2D 3.4 cm diameter cylinder with ε_r = 38.5 and σ= 0.85°S/m was imaged inside a homogeneous background medium of saline (ε_r = 77 and σ= 1.7°S/m). The algorithm utilized Marquardt regularization [Meaney et al. 2001b]. The 500 MHz permittivity and conductivity image pair shown in Figure 2 illustrates that such a target can be readily recovered.

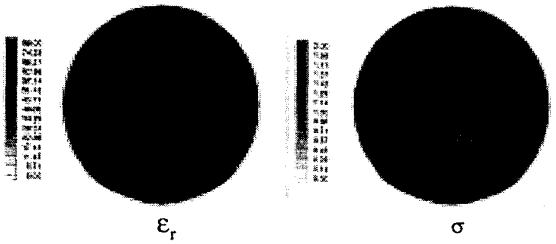

Fig. 2. 500 MHz reconstructed permittivity and conductivity images for a 3.4 cm diameter cylinder offset from the center. Electrical properties are 1/2 of the background properties.

An interesting and important observation can be made regarding the construction of the Jacobian matrix used to update the 2D property distribution at each iteration (by far the most time-consuming part of the algorithm). First the forward solution can be written in matrix form as:

$$[A]\{E\}=\{b\} \qquad (1)$$

where $[A]$ comprises the ∇^2+k^2 operator of the Helmholtz equation expressed as weighted residual integrations over the domain, $\{E\}$ is the electric field vector at all nodes in the 3D mesh and $\{b\}$ are the source terms. The Jacobian matrix used in computing the electrical property updates at each iteration is comprised of entries which are the derivatives of the electric fields at measurement sites with respect to the k^2 values at each of the reconstruction mesh nodes. They are formed by taking the derivative of equation (1) with respect to k_i^2 to form (after some re-arranging):

$$[A]\left\{\frac{\partial E}{\partial k_i^2}\right\}=-\left[\frac{\partial A}{\partial k_i^2}\right]\{E\} \qquad (2)$$

Note that only a small subset of $\left\{\frac{\partial E}{\partial k_i^2}\right\}$ is used in the Jacobian. This operation must be repeated for all transmitters. Multiplication of $\{E\}$ by $\left[\frac{\partial A}{\partial k_i^2}\right]$ essentially creates a vector with a simple weighting of the electric field values at sites in the 3D mesh near the i^{th} parameter mesh node. This vector is mostly zero except for elements corresponding to those weighting sites. If the electric field distribution over this very small zone can be considered nearly constant, the operation of multiplying $\{E\}$ by $\left[\frac{\partial A}{\partial k_i^2}\right]$ and solving for $\left\{\frac{\partial E}{\partial k_i^2}\right\}$ is essentially identical for all possible transmitters for the given i^{th} k^2 node. Thus, this operation (involving time-consuming matrix back substitutions) need only be performed for a single excitation, $\{E^1\}=\{1,1,1,\ldots 1\}^T$, and the $\left\{\frac{\partial E}{\partial k_i^2}\right\}$ terms for all transmitters can be constructed as simple weightings of the above result based on differences of the actual $\{E\}$ vectors for the transmitters. The errors introduced by forming the Jacobian in this manner are generally less than 1% and the time savings are significant. The number of matrix back substitutions at each iteration is NX × N where NX is the number of transmitters and N is the number of reconstruction parameters, respectively. For the current simulations, this amounts to 16°×°126°=°2016 back-substitutions. For the new approach, we need only perform the back-substitutions for a single transmitter, resulting in only 126 back-substitutions. This is a savings of 1890 back-substitutions, which corresponds to a reduction in computation time at each iteration of roughly 43 minutes to 2.2 minutes using an IBM RS/6000 43P model 260 workstation.

B. *Reduction of Phase-Wrapping Effect*

We have demonstrated that one of the most significant problems in imaging the breast in a high contrast medium (i.e. saline) is that the scattered field phases can easily undergo wrapping depending on the breast cross-sectional size, its permittivity contrast with the background and the operating frequency [Meaney et al. 2001c]. It was shown that when the percentage of measured scattered field phases exhibiting wrapping exceeded 50%, the image

reconstruction process diverges without dependence on a priori information or implementation of our phase unwrapping reconstruction algorithm. Interestingly, because of hardware constraints in our first prototype system, we could only utilize measurement data at the nine receivers opposite each transmitter. In fact, generally it was only these measurements that tended to be wrapped. In the simulations performed with this new 3D algorithm, we have also used measurement sites closer to each transmitter. Utilization of these data tends to reduce the overall percentage of scattered field phases which are wrapped. This has the net effect of facilitating convergence to a useful image for a breast phantom with a tumor inclusion which diverged when only the subset of nine receivers per transmitter was used. Figure 3 shows a plot of the unwrapped scattered phases for all fifteen receivers for a single transmitter for the case of an 11°cm diameter breast ($\varepsilon_r = 20$ and $\sigma = 0.2$°S/m) with a 2.5 cm diameter tumor inclusion ($\varepsilon_r = 56$ and $\sigma = 1.2$°S/m) offset to the right of center by 3 cm. For the case of the central nine measurements the percentage of wrapped phases exceeds 50% while the percentage is closer to the threshold when utilizing all fifteen measurement positions. The 500 MHz recovered permittivity and conductivity images using the two sets of receivers is shown in Figures 4a and b. In this case a coarse initial estimate of the property distribution was used. Even with this a priori information, the reconstruction using the 9 receivers was unable to reconstruct a meaningful image while its counterpart using 15 receivers reconstructed a good image.

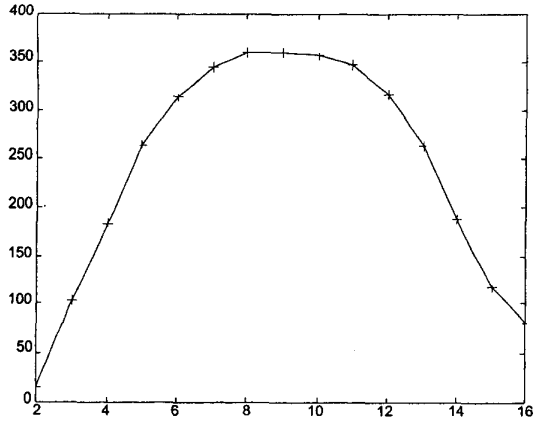

Fig.3. (a) Scattered unwrapped phases measured at the 15 receivers for a single transmitter at 500 MHz.

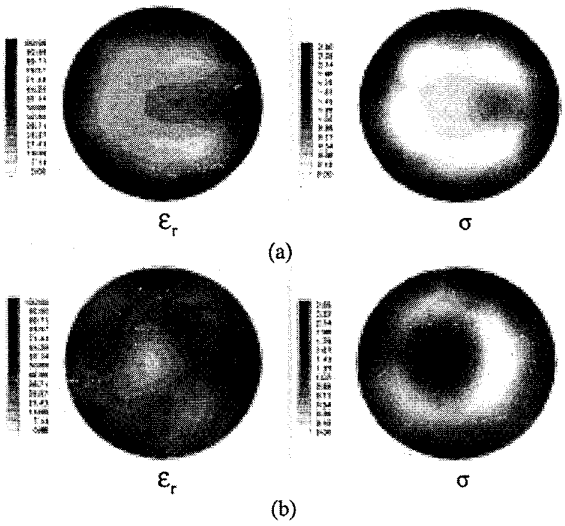

Fig.4. (a) 500 MHz reconstructed permittivity and conductivity images for the cases using (a) all 15 receiver sites per transmitter and (b) a subset of only the 9 central receiver sites.

IV. Conclusion

We have demonstrated in simulation that our new microwave imaging algorithm works for two single targets. We have incorporated ideas that dramatically reduce the computation time which is a primary limitation for 3D approaches. We have also shown that results where there is significant scattered field phase wrapping are consistent with previous 2D findings. These results are encouraging. However, the algorithm needs to be studied more thoroughly in terms of various imaging targets to assess improvements over previous 2D approaches.

Acknowledgement

This work was sponsored by NIH/NCI grant number R01 CA55034-09.

References

[1] Caorsi S, Massa A, Pastorino M, "A numerical solution to full-vector electromagnetic scattering by three-dimensional nonlinear bounded dielectrics," IEEE Transactions on Microwave Theory and Techniques, vol. 43, pp. 428-436, 1995.

[2] Semenov SY, Svenson RH, Bulyshev AE, Souvorov AE, Nazarov AG, Sizov YE, Pavlovsky AV, Borisov VY, Voinov BA, Simonova GI, Starostin AN, Posukh VG, Tatsis GP, Baranov VY, "Three-dimensional microwave tomography: experimental prototype of the system and vector Born reconstruction method," IEEE Transactions on Biomedical Engineering, vol. 46, pp. 937-946, 1999.

[3] Meaney PM, Paulsen KD, Geimer S, Haider S, Fanning MW, Quantification of 3D field effects during 2D microwave imaging, IEEE Transactions on Biomedical Engineering, 2001a (submitted).
[4] Meaney PM, Fanning MW, Li D, Poplack SP, Paulsen KD, "A clinical prototype for active microwave imaging of the breast," *IEEE Trans. Microwave Theory Tech.*, vol. 48, pp. 1841-1853, 2000.
[5] Paulsen KD, Meaney PM, Moskowitz MJ, Sullivan, Jr. JM, "A dual mesh scheme for finite element based reconstruction algorithms," IEEE Transactions on Medical Imaging, vol. 14, pp. 504-514, 1995.
[6] Meaney PM, Demidenko E, Yagnamurthy NK, Li D, Fanning MW, Paulsen KD, "A two-stage microwave image reconstruction procedure for improved internal feature extraction," Medical Physics, vol. 28, pp. 2358-2369, 2001b.
[7] Meaney PM, Paulsen KD, Pogue BW, Miga MI, "Microwave image reconstruction utilizing log-magnitude and unwrapped phase to improve high-contrast object recovery," IEEE Transactions on Medical Imaging, vol. 20, pp. 104-116, 2001c.